Vokasi Unesa Bulletin of Engineering, Technology and Applied Science (VUBETA)
https://journal.unesa.ac.id/index.php/vubeta
Vol. 3, No. 3, 2026, pp. 544~561 DOI: 10.26740/vubeta.v3i3.52684
ISSN: 3064-0768

Numerical Method for Solving Unsteady Squeezing Magnetohydrodynamic Eyring-Powell Fluid Model with Variable Thermophysical Properties

Bepo Adeyemi Ademola[1*], Oderinu Rasaq Adekola[2], Akindele Akintayo Oladimeji[3], Ogunniyi Oluyoola Dorcas[4], Oladapo Olayinka Akeem[5]
[1,2,3,4]Department of Pure and Applied Mathematics, Ladoke Akintola University of Technology, Ogbomoso, Oyo State, Nigeria
[5]Department of Mathematics, Obafemi Awolowo University, Ile-ife, Osun State Nigeria

Article Info

Article history:

Received April 09, 2026
Revised May 17, 2026
Accepted June 10, 2026

Keywords:

Magneto-hydrodynamic
Eyring-Powell fluid model
Squeezing flow
Variable thermo physical properties
Orthogonal polynomial

ABSTRACT

This investigation studies an unsteady squeezing magnetohydrodynamic flow of an Eyring–Powell fluid confined between two parallel plates with variable thermophysical properties, with an Arrhenius–type chemical reaction occurring simultaneously. The coupled nonlinear equations- the momentum one, then energy, and concentration too- are reshaped into dimensionless ordinary differential equations using similarity transformations, which kind of simplifies things, at least in the mathematical sense. After that, they craft a unified semi-numerical approach involving Chebyshev polynomials, a Galerkin weighted-residual framework, and Gauss–Legendre quadrature, so the numerical results can be obtained accurately without too much complication. They also provide a convergence analysis, which shows that stable solutions are reached at low polynomial order (N = 12), which is a good sign. Later, the authors cross-check the strategy against benchmark results reported by Ghadikolaei et al. (2017), and the matching outcomes support the methodis accuracy. In the results section, increasing electrical conductivity strengthens the Lorentz force and suppresses the velocity field, while higher thermal conductivity enhances the temperature distribution. Also, variable mass diffusivity thickens the concentration boundary layer, and if activation energy increases, the reaction rate slows, which then increases species concentration. Finally, they compute the skin friction coefficient, the Nusselt number, and the Sherwood number, which are used to quantify momentum, heat, and mass transfer, respectively. Overall, the Chebyshev–Galerkin scheme shows rapid convergence, reliable numerical stability, and good accuracy for nonlinear MHD non-Newtonian flow problems that include variable properties and reactive transport.

1. INTRODUCTION

Researchers study the behavior of electrically conductive fluids in magnetic fields in magnetohydrodynamics (MHD). These interactions occur in multiple systems containing liquid metals, plasma, electrolytes, polymeric fluids, and industrial transport systems that undergo major changes in momentum, heat, and mass transfer because of electromagnetic forces. Conventional MHD models link the Navier–Stokes equations to the Maxwell electromagnetic equations, showing how the Lorentz force affects velocity and temperature distributions in engineering systems such as cooling channels, nuclear reactors, electromagnetic pumps, lubrication devices, and polymer processing units [1]-[9]. Recent studies have enhanced this framework by investigating MHD flow of non-Newtonian fluids through porous media, showing how chemical reactions and nanoparticle transport affect flow patterns [10]-[12]. Researchers have studied peristaltic and oscillatory transport mechanisms through electromagnetic fields to understand their effects on

*Corresponding Author
Email: bepoadeyemi59@gmail.com

simultaneous heat and mass transfer in both industrial processes and human systems [13][14]. Researchers have expanded MHD flow analysis to include non-Newtonian fluids because most industrial fluids exhibit stress–strain behavior that does not comply with Newtonian theory. The Eyring–Powell fluid model stands as the most accepted non-Newtonian model because it demonstrates shear-thinning and shear-thickening behavior while maintaining Newtonian characteristics at low shear rates. Researchers have conducted extensive research on this model to study how variable viscosity and activation energy affect its behavior, particularly in nanofluid systems where Arrhenius-type reactions significantly influence concentration distribution [15]-[18]. Further studies have shown that heterogeneous–homogeneous chemical reactions strongly affect mass transfer characteristics in Powell–Eyring nanofluid flows, particularly in the presence of magnetic fields and porous media [19]-[21]. Advanced numerical techniques, such as spectral collocation methods, have also been applied to solve the highly nonlinear governing equations arising from MHD Eyring–Powell models, providing accurate predictions of velocity and thermal fields [22][23]. Squeezing flow between two parallel plates is another essential configuration used in hydraulic machinery, lubrication systems, microfluidic devices, and polymer extrusion processes. Recent studies on unsteady squeezing MHD flows have demonstrated that radiation and chemical reaction effects significantly influence heat transfer rates and flow stability in confined geometries [24]-[27]. Thermosolutal convection of Powell–Eyring fluids under magnetic fields has been shown to be a vital element controlling microchannel and microscale heat transfer systems [28][29]. Real industrial fluids display thermophysical property variations because their electrical conductivity and thermal conductivity depend on temperature, while their mass diffusivity depends on concentration. Studies have shown that incorporating rotation and variable property effects significantly changes flow characteristics, which improves thermal systems' predictive accuracy [30]-[33].

Table 1. Nomenclature of Symbols and Parameters

Nomenclature			
B	Non-uniform magnetic field	j_ω	the mass flux
B_0	uniform magnetic field	k	thermal conductivity
C	fluid concentration	k*	mean absorption coefficient
C_0	initial fluid concentration	l	initial distance between the plates
D_m	mass diffusion	q_ω	the wall heat flux
Q	heat generation/absorption parameter	u,v	velocity components
$Q*$	uniform volumetric heat generation/absorption coefficient fluid temperature	x,y	space coordinates
T	fluid temperature	δ_ω	temperature different
Greek symbols			
T_0	initial fluid temperature	α	characteristic parameter
R	radiation parameter	β	characteristic of the fluid
S	squeezing parameter	γ	chemical reaction parameter
Ha	Hartman number	μ	dynamic viscosity
Pr	Prandtl number	v	kinematic viscosity
Ec	Eckert number	σ	electrical conductivity of the fluid
Sc	Schmidt number	$\sigma*$	Stefan-Boltzman constant
Cf	Skin friction coefficient	ρ	fluid density
Nu_x	Nusselt number	τ, δ	Eyring- Powell fluid parameters
Sh	Sherwood number	θ	dimensionless temperature
Re_x	Reynolds number	ϕ	dimensionless concentration
C_p	specific heat capacity	φ_ω	the wall shear stress
C	characteristic of the fluid	ϑ	dimensionless variable

The Arrhenius activation energy determines chemical reaction velocity, which changes the species concentration distribution within the boundary layer of many reactive fluid systems. Recent computational investigations have confirmed that variable thermal conductivity and activation energy strongly influence nanofluid transport behaviour in MHD boundary layer flows [34]-[41]. Research on MHD flows, Eyring–Powell fluids, and squeezing configurations has been extensive, yet unsteady squeezing MHD Eyring–Powell flow with simultaneously variable thermophysical properties and Arrhenius chemical reaction effects remains largely unexplored. Previous studies used numerical techniques as separate methods because they treated Chebyshev polynomials, Galerkin weighted residual methods, and Gauss-Legendre quadrature as distinct tools, rather than developing a unified computational framework [42]-[49].

1.1. Research gap

A unified semi-numerical spectral framework to solve unsteady squeezing MHD Eyring–Powell flow equations involving highly nonlinear coupled equations, variable transport properties, and chemical reaction effects remains unachieved because a clear technological gap exists in this area of research.

1.2. Proposed solution

To address this gap, this study develops a hybrid semi-numerical scheme that combines Chebyshev polynomials with a Galerkin weighted-residual formulation and Gaussian quadrature integration into a single solution method. The governing nonlinear equations are transformed into dimensionless ordinary differential equations, which researchers discretize using shifted Chebyshev basis functions. Galerkin projection transforms the residual system into algebraic equations, while Gauss-Legendre quadrature provides accurate integral evaluation.

1.3. Main results obtained

The method demonstrates rapid convergence at low polynomial order (N = 12) and produces highly accurate results when compared with the benchmark solution of [36]. The analysis reveals that:

- Increasing electrical conductivity strengthens the Lorentz force and suppresses velocity,
- Enhanced thermal conductivity raises temperature distribution,
- Variable mass diffusivity enlarges concentration boundary layer thickness,
- Higher activation energy reduces reaction rate and increases species concentration.

Engineering quantities, including the skin friction coefficient, Nusselt number, and Sherwood number, are evaluated to characterize momentum, heat, and mass transfer.

1.4. Research contributions of this study

This work contributes to knowledge in the following ways:

- Development of a unified Chebyshev–Galerkin–Gauss Legendre quadrature semi-numerical method for nonlinear MHD non-Newtonian flow problems.
- First investigation of unsteady squeezing MHD Eyring–Powell flow with simultaneously variable thermophysical properties and an Arrhenius chemical reaction.
- Demonstration of rapid convergence and numerical stability at a low discretization level (N = 12).
- Validation of the proposed method with established results from the literature.

Detailed analysis of how magnetic field, squeezing motion, variable conductivity, diffusivity, and activation energy influence velocity, temperature, and concentration profiles.

2. MATHEMATICAL FORMULATION OF THE PROBLEM

The study investigates the unsteady squeezing flow of magnetohydrodynamic (MHD) Eyring-Powell fluid model, characterized by variable thermophysical properties, emphasizing the alignment of the velocity field $u(x) = ax$ along the *x*–axis direction which form the basis of this paper in the presence of a non-uniform magnetic field $B(x) = (1-\alpha t)^{-\frac{1}{2}}$ between two infinite parallel plates separated by a distance $\alpha(x) = (1-\alpha t)^{-\frac{1}{2}}$ and investigating the characteristics of heat transfer and the flow of this Eyring-Powell fluid [37]. The analysis was based on the following assumptions in this case:

- The initial distance between the plates at time t and the characteristic parameter of the squeezing motion of the plate with dimension of the inverse time.
- The effects of thermal radiation, heat generation/ absorption, Lorentz force, and Joule heating.
- Variable thermophysical properties such as electrical conductivity, thermal conductivity, and thermal diffusivity were also considered

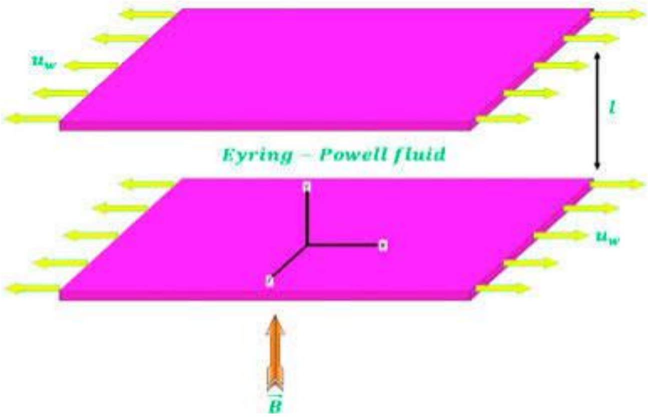

Figure 1. Geometry of the problem

.

$$\sigma(T) = \sigma_0(1 + \varepsilon_2(\frac{T-T_0}{T_1-T_0}))^n) \tag{1}$$

Equation (1) describes the electrical conductivity $\sigma(T)$ of a material as a function of temperature (T). The equation suggests that electrical conductivity increases nonlinearly with temperature; justify the claim with experimental literature.

$$k(T) = k(1 + \varepsilon_4\left(\frac{T-T_0}{T_1-T_0}\right)) \tag{2}$$

Equation (2) describes the thermal conductivity (k) of a material as a function of temperature (T). The equation suggests that thermal conductivity increases linearly with temperature [36].

$$D(C) = D_m(1 + \left(\frac{T-T_0}{T_1-T_0}\right)) \tag{3}$$

This equation (3) describes the diffusion coefficient (D) of a substance as a function of concentration (C). The equation suggests that the diffusion coefficient increases linearly with concentration. The chemical term in fluid dynamics represents the effects of chemical reactions on fluid's properties and behaviors [36].

The nonlinear differential equations that model this problem are divided into two categories of momentum equations and energy equations that are given below:

$$\frac{\partial u}{\partial x} + \frac{\partial v}{\partial y} = 0 \tag{4}$$

$$\frac{\partial u}{\partial t} + u\frac{\partial u}{\partial x} + v\frac{\partial u}{\partial y} = \frac{-1}{\rho}\frac{\partial \rho}{\partial x} + \left(v + \frac{1}{\rho\beta c}\right)\left(\frac{\partial^2 u}{\partial x^2} + \frac{\partial^2 u}{\partial y^2}\right) - \frac{-1}{3\rho\beta c^3}\frac{\partial}{\partial x}[(2\left(\frac{\partial u}{\partial x}\right)^2 + 2\left(\frac{\partial v}{\partial y}\right)^2 + \left(\frac{\partial u}{\partial y} + \frac{\partial v}{\partial x}\right)^2)\frac{\partial u}{\partial x})] - \frac{1}{6\rho\beta c^3}\frac{\partial}{\partial y}[(2(\frac{\partial v}{\partial x})^2 + 2(\frac{\partial v}{\partial y})^2\left(\frac{\partial u}{\partial y} + \frac{\partial v}{dx}\right)^2\left(\frac{\partial u}{\partial y} + \frac{\partial v}{\partial x}\right)] - \frac{\sigma(T)B_0}{\rho(1-\alpha t)}u \tag{5}$$

$$\frac{\partial v}{\partial t} + u\frac{\partial v}{\partial x} + v\frac{\partial v}{\partial y} = \frac{-1}{\rho}\frac{\partial \rho}{\partial x} + \left(v + \frac{1}{\rho\beta c}\right)\left(\frac{\partial^2 v}{\partial x^2} + \frac{\partial^2 v}{\partial y^2}\right) - \frac{-1}{6\rho\beta c^3}\frac{\partial}{\partial x}[(2(\frac{\partial u}{\partial x})^2 + 2(\frac{\partial v}{\partial y})^2 + (\frac{\partial u}{\partial y} + \frac{\partial v}{\partial x})^2)(\frac{\partial u}{\partial y} + \frac{\partial v}{\partial x})] - \frac{1}{3\rho\beta c^3}\frac{\partial}{\partial y}[(2(\frac{\partial u}{\partial x})^2 + 2(\frac{\partial v}{\partial y})^2\left(\frac{\partial u}{\partial y} + \frac{\partial v}{dx}\right)^2\left(\frac{\partial u}{\partial y} + \frac{\partial v}{\partial x}\right)] \tag{6}$$

$$\frac{\partial T}{\partial t} + u\frac{\partial T}{\partial t} + v\frac{\partial T}{\partial t} = \frac{k}{\rho c_\rho}\frac{\partial}{\partial y}\left(k(T)\frac{\partial T}{\partial y}\right) + \frac{1}{\rho c_\rho}\frac{\partial q_r}{\partial y} + \frac{Q^*}{\rho c_\rho}(T - T_0) + \frac{\sigma(T)B^2}{\rho c_\rho}u^2 \tag{7}$$

$$\frac{\partial C}{\partial t} + u\frac{\partial C}{\partial t} + v\frac{\partial C}{\partial t} = \frac{\partial}{\partial y}\left(D(C)\frac{\partial C}{\partial y}\right) + K_r(C - C_0)(\frac{T}{T_0})^m e^{-\frac{E}{kT}} \tag{8}$$

u and v are the component of the velocity in the direction of x and y, respectively, ρ is the fluid density, V is the kinematic viscosity, q_r is thermal radiation, E_a is activation energy, β and c are characteristics of Eyring-Powell fluid, B_0 is the uniform magnetic field, $\sigma(T)$ is the variable electrical conductivity, k(T) is the variable thermal conductivity of the fluid, D(C) is the variable thermal diffusivity, c_ρ is the specific heat capacity, σ^* is the Stefan-Boltzmann constant, T is the fluid temperature and T_0 is the referenced fluid temperature, k^* is the mean absorption coefficient, ε_2 is the electrical conductivity parameter, ε_4 is the thermal conductivity parameter, ε_6 is the thermal diffusivity parameter, Q^* is the uniform volumetric heat generation/absorption coefficient, D_m is the mass diffusion, k_r is the Arrhenius constant, q_r is the radiative heat flux, C and c_0 are respectively the concentration and referenced concentration of the fluid.
Also, the appropriate boundary conditions for the above equations are given according to the assumptions and considered conditions in the problem as follows:
The boundary conditions for the equation are defined as follows:

$$u = 0, v = v_w = \frac{\partial a}{\partial t}, T = T_0, C = C_0, \alpha t\ \ y = \alpha(t), v = \frac{\partial u}{\partial y} = \frac{\partial T}{\partial y} = \frac{\partial C}{\partial y} = 0, as\ y = 0 \tag{9}$$

Follow changes are applied to made velocity $f'(\eta)$, temperature $\theta(\eta)$, and concentration $\emptyset(\eta)$, functions dimensionless:

$$\eta = \frac{y}{l(1-\alpha t)^{\frac{1}{2}}}, u = \frac{\alpha x}{2(1-\alpha t)}\frac{\partial f(\eta)}{\partial \eta}, v = \frac{\alpha l}{2(1-\alpha t)^{\frac{1}{2}}}f(\eta), \theta = \frac{T-T_0}{T_1-T_0}, \emptyset = \frac{C-C_0}{C_1-C_0} \tag{10}$$

Where vorticity is given as:

$$\omega = (\frac{\partial v}{\partial x} - \frac{\partial u}{\partial y}) \tag{11}$$

By cross-differentiating Equation (5) and Equation (6) with Equation (10) and Equation (11), the PDEs are changed to ODEs as:

$$(1+\tau)f^{iv} - S(f''' + 3f'' + f'f'' - ff'') - \tau\delta(2f''(f'')^2 + (f'')^2 f^{iv}) - Ha^2 f''\,(1+\varepsilon_2\theta)^n = 0 \quad (12)$$

So, nonlinear differential equations governing the problem after making Equations (7)-(9) dimensionless and changing PDEs to ODEs using Equations (10) are given as follows:

$$\left(1+\varepsilon_4\theta+\frac{4}{3}R\right)\theta'' + \varepsilon_4\theta'^2 + PrS(f\theta' - \eta\theta' + Q\theta) + PrHa^2Ecf'^2(1+\varepsilon_2\theta)^n = 0 \quad (13)$$

$$(1+\varepsilon_6\emptyset)\emptyset'' + \varepsilon_6\emptyset'^2 + ScS(f\emptyset' - \eta\emptyset') - Sc\gamma(\left(1-\delta_\omega\theta\right)^m e^{-\left(\frac{E}{1+\delta_\omega\theta}\right)}\Big)\emptyset = 0 \quad (14)$$

The dimensionless numbers and parameters are as follows:
$\tau = \frac{1}{\mu\beta C}$ and $\delta = \frac{\alpha^2 x^2}{8\beta C^2(1-\alpha t)^3}$ are the Eyring-Powell fluid parameters, $S = \frac{\alpha l}{2\upsilon}$ is the squeezing parameter, it is worth mentioning when the plates moving apart $(S > 0)$ and when the plates collapsing together $(S < 0)$, $Ha = \sqrt{\frac{\sigma}{\mu}}B_0 l$ is the Hartman number (magnetic field parameter), $\frac{\partial q_r}{\partial y} = -\frac{16\sigma T_0^3}{3k^*}\frac{\partial^2 T}{\partial y^2}$ is the radiative heat flux parameter, $\frac{E_a}{KT} = \frac{E}{1+\delta_\omega\theta}$ is the dimensionless activation energy parameter,$R = \frac{4\sigma^* T_0^3}{kk^*}$ is the radiation parameter, $Q = \frac{2Q^*(1-\alpha t)}{\alpha\rho C_\rho}$ is the heat generation $(Q > 0)$ or absorption $(Q < 0)$ parameter, $Pr = \frac{\mu C_\rho}{k}$ is the Prandtl number, $Ec = \frac{(u(x))^2}{C_\rho T_0}$ is the Eckert number, $Sc = \frac{\upsilon}{D_m}$ is the Schmidt number $\gamma = \frac{l^2 K_r}{\upsilon}$ is the chemical reaction parameter where in, $(\gamma > 0)$ the destructive chemical reaction and $(\gamma < 0)$, represents the generative chemical reaction.
In the following, using Equation (10) in Equation (9), the boundary conditions of Equations (12-14) are as follows:

$$f(\eta) = 0, f''(\eta) = 0, \theta(\eta) = 0, \emptyset(\eta) = 0, at\ \eta = 0$$
$$f'(\eta) = 0, f(\eta) = 1, \theta(\eta) = 1, \emptyset(\eta) = 1, at\ \eta = 1 \quad (15)$$

3. SKIN FRACTION COEFFICIENT (Cf), LOCAL NUSSELT NUMBER (Nu) AND SHERWOOD NUMBER (Sh)

They are defined as follows:

$$Cf = \frac{\varphi_\omega}{\rho\upsilon\omega_2} \quad (16)$$
$$Nu = \frac{lq_\omega}{k(T_1 - T_0)} \quad (17)$$
$$Sh = \frac{lj_\omega}{D_{m(C_1 - C_0)}} \quad (18)$$

That φ_ω the wall shear stress, q_ω the wall heat flux and the mass flux are respectively equal to:

$$\varphi_\omega = \{\left(\mu + \frac{1}{\beta c}\right)\frac{\partial u}{\partial y} - \frac{1}{6\beta c^3}(\frac{\partial u}{\partial y})^2\}_{y=\alpha(t)} \quad (19)$$
$$q_\omega = \{-k\frac{\partial T}{\partial y} - \frac{16\sigma^* T_0^3}{3k^*}\frac{\partial T}{\partial y}\}_{y=\alpha(t)} \quad (20)$$
$$j_\omega = \{D_m\frac{\partial C}{\partial y}\}_{y=\alpha(t)} \quad (21)$$

Finally, by replacing Equation (19)-(21) in Equation (16)-(18), surface drag force, heat transfer rate and mass transfer rate are as follows:

$$Re_x\frac{l^2}{x^2}Cf = (1-\tau)f''(1) - \frac{\tau\delta}{3}(f''(1))^3 \quad (22)$$
$$(1-\alpha t)^{\frac{1}{2}}Nu = -(1+\frac{4}{3}R)\theta'(1) \quad (23)$$
$$(1-\alpha t)^{\frac{1}{2}}Sh = -\emptyset'(1) \quad (24)$$

That $Re_x = \frac{\alpha l x(1-\alpha t)^{\frac{1}{2}}}{2\upsilon}$ is the local Reynolds number.

.

4. NUMERICAL METHOD

4.1 Semi-numerical approximation using Chebyshev polynomials

The governing nonlinear differential equation is considered on a finite domain subject to prescribed boundary conditions:

$$L(u) = 0, x \in [-1,1] \tag{25}$$

The unknown function is approximated using a finite series of Chebyshev polynomials:

$$u_N(\eta) = \sum_{j=0}^{N} a_j T_j(\eta) \tag{26}$$

The governing equation is enforced at Chebyshev–Gauss–Lobatto points:

$$\eta_k = cos\left(\frac{k\pi}{N}\right), \qquad k = 0,1, \dots., N \tag{27}$$

Derivatives of the approximate solution are computed using Chebyshev differentiation matrices:

$$u'(\eta_k) = \sum_{j=0}^{N} D_{kj} u(\eta_j) \tag{28}$$

Substituting the approximate solution into the governing equation yields the residual:

$$R(\eta) = L(u_N(\eta)) \tag{29}$$

The residual R(η) measures the deviation of the approximate solution from the exact solution. The formulation is completed by enforcing the boundary conditions together with a collocation strategy. The boundary conditions generate four algebraic equations, while the residual is forced to vanish at selected Gauss–Legendre collocation points within the domain. This leads to

$$R(\eta_i) = 0 \qquad i = 1,2,3, \tag{30}$$

Where η_i are Gauss–Legendre nodes mapped onto the interval [0,1]. Consequently, the continuous boundary value problem is reduced to a system of seven nonlinear algebraic equations in the seven unknown coefficients $a_0,\ a_1, \dots, a_6$. Because the resulting system is strongly nonlinear, we obtain a numerical solution using an iterative nonlinear solver implemented in Maple (fsolve), which computes the spectral coefficients simultaneously.

4.2 Boundary condition enforcement

The boundary conditions in equation (15) are incorporated into the system of algebraic equations AX=b using an enforcement technique, depending on the nature of the condition. By replacing row at boundary collocation points with values from equation (14) gives:

$$R_B(x,y) = \aleph[f_N(x,y) - f_{BC}(x,y)^2] \tag{31}$$

4.3 Numerical Implementation oundary condition enforcement

Let us consider dimensionless models of equations (12), (13), and (14); the resulting system of nonlinear algebraic equations was solved numerically using an iterative solver implemented in Maple. The solver computes the unknown spectral coefficients simultaneously, ensuring that both the governing equation and boundary conditions are satisfied in an approximate sense. In order to solve (12) using the Chebyshev polynomial, the Chebyshev terms of the polynomials of the first kind are obtained as

$$\left.\begin{aligned}
T_0^*(x) &= 1\\
T_1^*(x) &= 2\eta\\
T_2^*(x) &= 4\eta^2 - 2\\
T_3^*(x) &= 8\eta^3 - 8\eta\\
T_4^*(x) &= 16\eta^4 - 40\eta^2 + 12\\
T_5^*(x) &= 32\eta^5 - 144\eta^3 + 88x\\
T_6^*(x) &= 64\eta^6 - 488\eta^4 + 476\eta^2 - 120
\end{aligned}\right\} \tag{32}$$

Assuming a trial function of the form:

$$y(\eta) = \sum_{i=0}^{6} a_i T_i^* \tag{33}$$

where a_i are constants to be determined, substituting equation (32) into (33)

$$\begin{aligned} y(\eta) &= a_0 + a_1(4\eta-2) + a_2\left(4(2\eta-1)^2-1\right) + a_3\left(8(2\eta-1)^3-8\eta+4\right) \\ &+ a_4\left(16(2\eta-1)^4-12(2\eta-1)^2+1\right) + a_5(32(2\eta-1)^5-32(2\eta-1)^3 \\ &+12\eta-6) + a_6\left(64(2\eta-1)^6-80(2\eta-1)^4+24(2\eta-1)^2-1\right) \end{aligned} \tag{34}$$

and the equation given is,

$$R = (1+\tau)\frac{\partial^4 y}{\partial x^4} - S(\eta(\frac{\partial^3 y}{\partial x^3} + 3\frac{\partial^2 y}{\partial x^2} + \frac{\partial y}{\partial x}\frac{\partial^2 y}{\partial x^2} - y\frac{\partial^3 y}{\partial x^3}) - \tau\delta(2\frac{\partial^2 y}{\partial x^2}(\frac{\partial^3 y}{\partial x^3})^2 + \frac{\partial^4 y}{\partial x^4}(\frac{\partial^2 y}{\partial x^2})^2 - Ha^2\frac{\partial^2 y}{\partial x^2} \tag{35}$$

Substituting (34) into (35), the residual (R) gives,

$$422.4a_4 + 4224a_5\eta + 1.1a_6(23040\eta^2 - 11712) + 7.2a_3 + 57.6a_4\eta + 0.15a_5(1920\eta^2 - 864) + 0.15a_6(7680\eta^3 - 11712\eta) + 35.9992a_2 + 215.9952a_3\eta + 4.4999a_4(192\eta^2 - 80) + 4.4999a_5(640\eta^3 - 864\eta) + 4.4999a_6(1920\eta^4 - 5856\eta^2 + 952) + 1.5\big(2a_1 + 8a_2 + a_3(24\eta^2 - 8) + a_4(64\eta^3 - 80\eta) + a_5(160\eta^4 - 432\eta^2 + 88)a_6(384\eta^5 - 1952\eta^3 + 952\eta)\big)\big(8a_2 + 48a_3\eta + a_4(192\eta^2 - 80) + a_5(640\eta^3 - 864\eta) + a_6(1920\eta^4 - 5856\eta^2 + 952)\big) - 1.5\big(48a_3 + 384a_4\eta + a_5(1920\eta^2 - 864) + a_6(7680\eta^3 - 11712\eta)\big)\big(a_0 + 2a_1\eta + a_2(4\eta^2 - 2) + a_3(8\eta^3 - 8\eta) + a_4(16\eta^4 - 40\eta^2 + 12) + a_5(32\eta^5 - 144\eta^3 + 88\eta) + a_6(64\eta^6 - 488\eta^4 + 476\eta^2 - 120)\big) + 0.02(8a_2 + 48a_3\eta + a_4(192\eta^2 - 80) + a_5(640\eta^3 - 864\eta) + a_6(1920\eta^4 - 5856\eta^2 + 952))(48a_3 + 384a_4\eta + a_5(640\eta^3 - 864\eta) + a_6(1920\eta^4 - 5856\eta^2 + 952))(48a_3 + 384a_4x + a_5(1920\eta^2 - 864) + a_6(7680\eta^3 - 11712\eta))^2 + 0.01(8a_2 + 48a_3\eta + a_4(192\eta^2 - 80) + a_5(640\eta^3 - 864\eta) + a_6(1920\eta^4 - 5856\eta^2 + 952))^2(384a_4 + 3840a_5\eta + a_6(23040\eta^2 - 11712)) \tag{36}$$

Equation (36) represents the residual equation obtained using the sixth-order Chebyshev polynomial approximation. The boundary conditions were imposed on the trial function given in Equation (33), after which the residual function was evaluated. In the weighted residual approach, the residual function is multiplied by a weighting function and enforced to Truncate at selected collocation points within the computational domain $0 \le x \le 1$. In this study, the approximate solution itself was chosen as the weighting function. Hence,

$$F(\eta) = w(\eta)R(\eta) \tag{37}$$

where

$$w(\eta) = y(\eta) \tag{38}$$

and $R(x)$ denotes the residual function. Substituting the weighting function into the residual equation gives

$$F(\eta) = y(\eta)R(\eta) \tag{39}$$

The resulting expression was then evaluated at selected collocation points in the interval $0 < x < 1$ producing a system of nonlinear algebraic equations. Solving these equations simultaneously yields the unknown coefficients of the Chebyshev polynomial approximation.

$$\begin{aligned} &a_0 = -9.422098208, a_1 = 13.70217183, a_2 = -5.97645105, \\ &a_3 = 2.748503404, a_4 = 0.2553004773, a_5 = 0.05018541391, \\ &a_6 = 0.04662019774 \end{aligned} \tag{40}$$

By substituting the computed constants obtained from Equation (40) into the trial function given in Equation (34), the approximate solution for the sixth-order Chebyshev polynomial is obtained for the velocity profile as:

$$f_6(\eta) = -0.000330898616 0 + 2.01783605\eta - 7.26849821\eta^2 + 14.144192887\eta^3 - 12.96718442\eta^4 + 5.54822583\eta^5 - 0.80543001\eta^6 \quad (41)$$

By applying the same procedure described in Equations (12), the resulting algebraic system leads to the solution for the temperature, is given in Equation (13) as:

$$\theta_6(\eta) = 0.00000124 - 0.03792144\eta - 0.1986472\eta^2 - 0.21400538\eta^3 - 0.14211609\eta^4 - 0.05849761\eta^5 - 0.00639412\eta^6 \quad (42)$$

Similarly, by following the same computational procedure for Equations (12) to (14), the governing equations for the concentration fields are reduced to algebraic systems. Solving these systems yields the solutions given in Equation (14) as:

$$\phi_6(\eta) = 0.95272406 + 0.00632185\eta + 0.01894277\eta^2 + 0.02851644\eta^3 - 0.02218490\eta^4 - 0.01211633\eta^5 - 0.00919421\eta^6 \quad (43)$$

5. RESULT AND DISCUSSION

After validating the numerical method through comparison, error analysis, and convergence assessment in Table 2-Table 4, the physical behavior of the flow, temperature, and concentration fields under various parameters is illustrated in Figure 2 – Figure 12. This section presents numerical results in figures and tables obtained using combined Chebyshev polynomial and Galerkin methods with Gauss-Legendre quadrature to solve the nonlinear differential equations (12)-(14) with boundary conditions specified in (15). The study demonstrates how different dimensionless numbers and parameters impact three profiles which include the velocity profile $f'(\eta)$ and the temperature profile $\theta(\eta)$ and the concentration profile $\phi(\eta)$. The study shows how these parameters impact three factors, which include the skin friction coefficient, the local Nusselt number, and the local Sherwood number.

Figure 2 and Figure 3 present the influence of the squeezing parameter on the velocity and temperature distributions, respectively. Figure 2 shows that increasing the squeezing parameter initially reduces the fluid velocity within the boundary layer region. This reduction occurs because stronger squeezing compresses the fluid layers, increasing flow resistance and limiting fluid movement near the surface. The imposed compression restricts the mobility of fluid particles, which consequently reduces the velocity magnitude. As the squeezing effect becomes stronger beyond a certain level, the velocity profile begins to increase. This behavior is attributed to the enhanced pressure-driven motion produced by the moving boundaries. At higher squeezing intensities, the confined fluid is forced to accelerate outward to conserve mass within the narrowing channel, increasing flow momentum and subsequently raising the velocity distribution.

Figure 3 illustrates the effect of the squeezing parameter on the temperature distribution. The temperature profile increases as the squeezing parameter increases. The compression generated by wall motion decreases the spacing between fluid molecules, which intensifies molecular interactions and internal friction within the fluid. These processes enhance thermal energy generation while simultaneously reducing heat diffusion away from the surface. Consequently, thermal energy accumulates within the fluid, resulting in higher temperature distributions and gradually converging temperature profiles away from the wall.

The influence of the Eyring–Powell fluid parameter on the velocity distribution is illustrated in Figure 4. The velocity profile initially decreases before reaching a minimum value and then increases farther from the surface. The initial reduction in velocity occurs because variations in the Eyring–Powell fluid parameter modify the fluid's non-Newtonian characteristics, effectively increasing resistance to deformation within the boundary layer. This increased resistance weakens fluid motion near the wall and reduces velocity. As the distance from the surface increases, the influence of viscous resistance diminishes while inertial effects become more significant. This allows the fluid to recover momentum, resulting in an upward trend in the velocity profile. This behavior reflects the shear-dependent nature of Eyring–Powell fluids, in which viscosity changes with the rate of deformation, altering momentum transport within the flow region. The effect of the Hartmann number on the velocity distribution is presented in Figure 5. The figure shows that increasing the Hartmann number reduces fluid velocity throughout the flow domain. This occurs because the applied magnetic field generates an electromagnetic resistive force within the electrically conducting fluid. The induced Lorentz force acts opposite to the direction of motion, suppressing fluid movement and increasing flow resistance. As a result, stronger magnetic field intensity produces greater damping of the velocity field.

Figure 6 illustrates the influence of the Prandtl number on the temperature distribution. Increasing the Prandtl number reduces the thermal boundary layer thickness and modifies the temperature profile within the fluid. This behavior occurs because a higher Prandtl number corresponds to lower thermal diffusivity, meaning heat diffuses more slowly than momentum. As a result, thermal energy becomes concentrated near the surface, producing higher temperature gradients and altering the temperature distribution within the flow region. Figure 7 presents the effect of the Eckert number on the temperature field. The temperature distribution increases with increasing Eckert number due to enhanced viscous dissipation. Higher Eckert number values indicate stronger conversion of kinetic energy into internal thermal energy through fluid friction. This process intensifies molecular interactions and generates additional heat within the fluid, thereby increasing the overall temperature distribution.

Figure 8 shows the variation of concentration with the Schmidt number. An increase in the Schmidt number results in a higher concentration profile within the boundary layer. This phenomenon arises because larger Schmidt number values correspond to lower mass diffusivity. Consequently, species diffusion becomes weaker, reducing the rate at which concentration spreads away from the surface and leading to thicker concentration accumulation near the wall. Figure 9 illustrates the effect of the chemical reaction parameter on the concentration distribution. The concentration decreases when destructive chemical reactions dominate because reactive species are consumed during the reaction process. In contrast, generative reactions promote species production or increase concentration levels. Therefore, stronger destructive reactions reduce species concentration, whereas weaker or generative reactions enhance concentration within the fluid. Figure 10 presents the influence of the Arrhenius activation energy parameter on temperature and the reaction process. Increasing activation energy reduces the reaction rate because reacting molecules require more energy to overcome the energy barrier. As a result, the reaction proceeds more slowly, allowing a larger amount of unreacted species to remain within the fluid. This reduced reaction rate weakens species consumption and contributes to an increase in the temperature distribution due to reduced energy loss associated with rapid chemical transformation.

Figure 11 illustrates the influence of the power law index on the concentration distribution. Increasing values of the power law index enhance the concentration profile throughout the boundary layer. This behavior is associated with changes in the fluid rheological properties, which modify the transport characteristics of diffusing species. Higher values of the power law index alter the reaction kinetics and reduce the effective rate of species consumption within the flow. Consequently, more solute particles remain in the fluid region, increasing concentration levels that extend across the boundary layer. Figure 12 presents the effect of the variable diffusivity parameter on the concentration distribution. The results indicate that increasing the variable diffusivity parameter enhances the concentration profile. This occurs because higher diffusivity improves solute particles' ability to spread from the surface into the surrounding fluid. Enhanced mass diffusion promotes stronger species transport, expanding the concentration boundary layer. As a result, concentration levels increase and persist throughout a larger portion of the flow region.

Table 2. Comparison of f(η) between (Ghadikolaei et al., 2017) and Current Method solution

H	Ghadikolaei *et al 2017* Ref [37]	Ghadikolaei *et al 2017* Ref [37]	Present Method N=12
0.0	0.00000000	0.00000000	0.00000000
0.1	0.13570349	0.13586036	0.15570904
0.2	0.26993918	0.27024429	0.30764648
0.3	0.40111409	0.40154944	0.45212858
0.4	0.52737667	0.52791339	0.58564656
0.5	0.64646613	0.64706222	0.70494319
0.6	0.75553451	0.75613223	0.80709290
0.7	0.85092861	0.85145329	0.88955017
0.8	0.92791395	0.92828058	0.95020706
0.9	0.98031233	0.98045878	0.98741594
1.0	1.00000000	1.00000000	1.00000000

.

Table 3. Comparison of θ(η) between (Ghadikolaei et al., 2017) and Current Method solution

H	Ghadikolaei *et al 2017* Ref [37]	Ghadikolaei *et al 2017* Ref [37]	Present Method N=12
0.0	1.24057491	1.24436958	1.00000000
0.1	1.23757897	1.24136511	0.887364215
0.2	1.23245465	1.23245465	0.773915482
0.3	1.21421461	1.21793614	0.665028917
0.4	1.19460186	1.19826972	0.563417804
0.5	1.17042909	1.17402303	0.470842931
0.6	1.14232106	1.14579471	0.387991602
0.7	1.11087683	1.11411598	0.314611893
0.8	1.07657820	1.07933042	0.249722348
0.9	1.03967242	1.04145177	0.191736521
1.0	1.00000000	0.99999999	0.000000000

Table 4. Comparison of ϕ(η) between (Ghadikolaei et al., 2017) and Current Method solution

s	Ghadikolaei *et al 2017* Ref [37]	Ghadikolaei *et al 2017* Ref [37]	Present Method N=12
0.0	0.95272406	0.95279202	0.95279202
0.1	0.95320035	0.95326834	0.95326834
0.2	0.95462834	0.95469642	0.95469642
0.3	0.95700552	0.95707374	0.95707374
0.4	0.96032813	0.96039646	0.96039646
0.5	0.96459176	0.96466003	0.96466003
0.6	0.96979240	0.96985996	0.96985996
0.7	0.97592789	0.97599285	0.97599285
0.8	0.98300000	0.98305768	0.98305768
0.9	0.99101744	0.99105727	0.99105727
1.0	1.00000000	1.00000000	1.00000000

The functions $f(\eta)$, $\theta(\eta)$, and ϕ (η) presented in Table 2–Table 4 are kind of compared with the benchmark outcomes given by Ghadikolaei *et al.* (2017) to check if the proposed numerical scheme is accurate enough. Overall, the results look very consistent through the whole computational span [0,1] so, it confirms the reliability of the Chebyshev–Galerkin–Gauss–Legendre quadrature. At the boundary points, exact agreement shows up, and at the intermediate nodal locations there are only tiny, almost negligible, mismatches.

The comparison also indicates that stable, grid-independent solutions are reached when the polynomial order is set to N=12. If the truncation order is pushed higher than that, there is basically no noticeable improvement, which suggests rapid convergence and good numerical sturdiness of the spectral approach. This close match with the reference solution means the semi-numerical scheme, as presented, provides an efficient and highly accurate way to handle the governing nonlinear system.

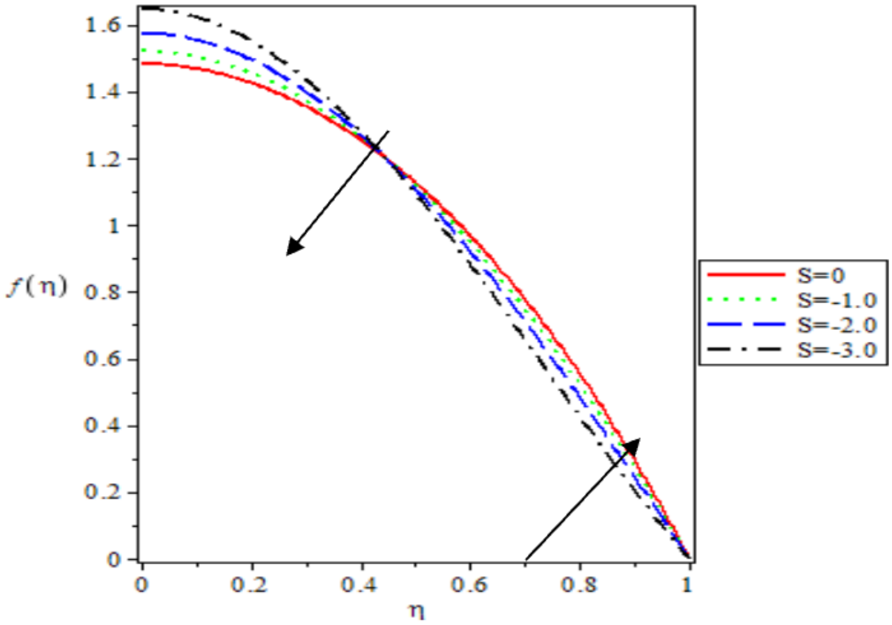

Figure 2. Influence of S on velocity profile

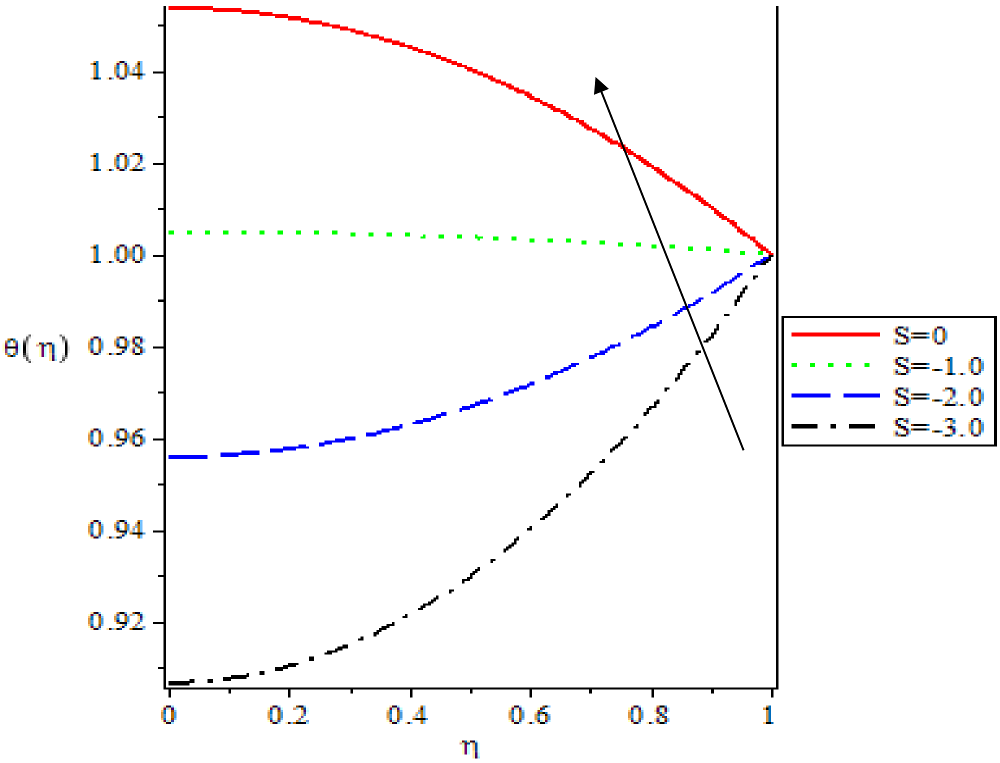

Figure 3. Influence of S on temperature profile

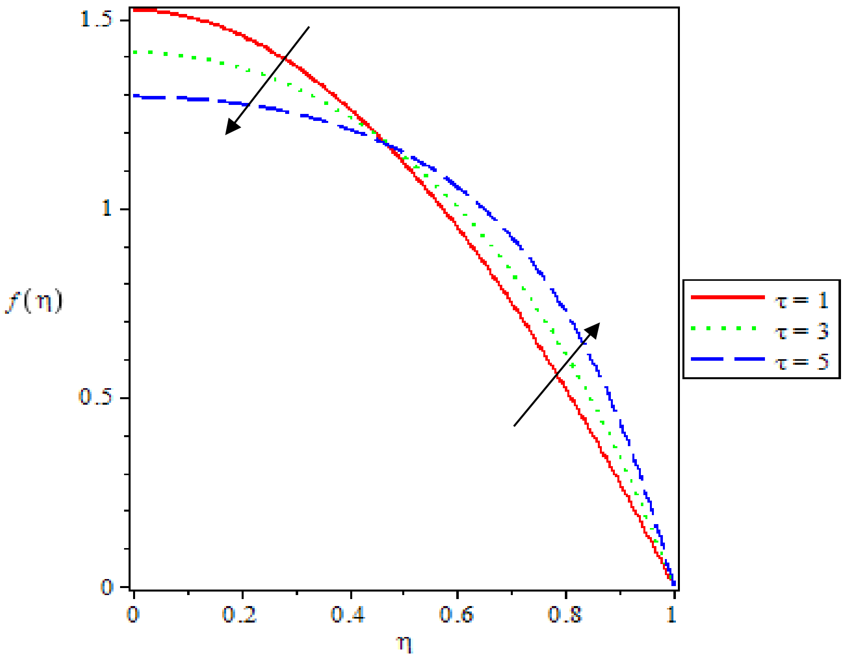

Figure 4. Influence of τ on velocity profile

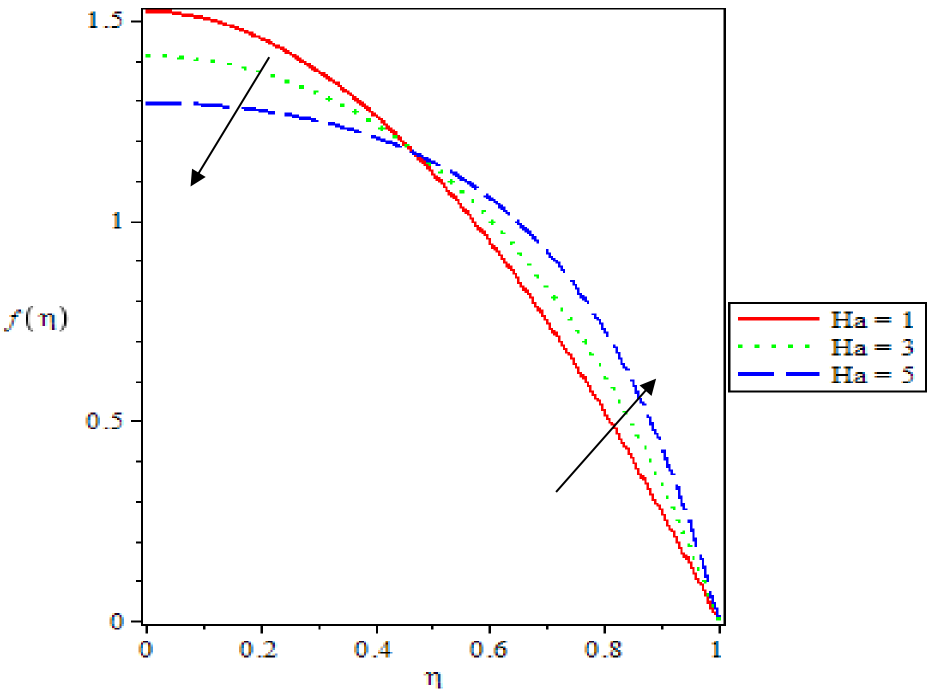

Figure 5. Influence of Ha on velocity profile

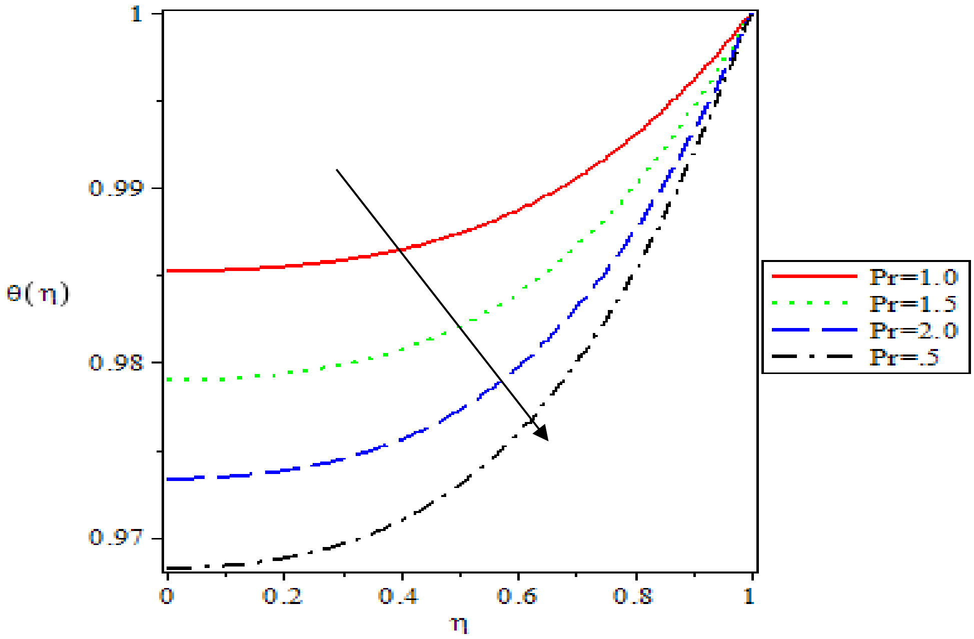

Figure 6. Influence of Pr on temperature profile

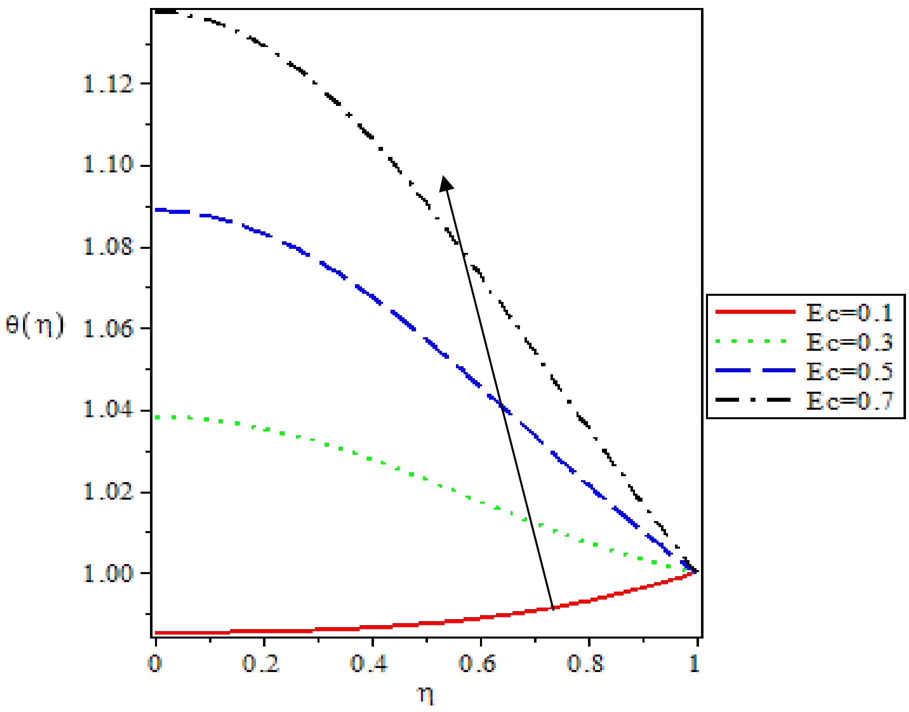

Figure 7. Influence of Ec on concentration profile

.

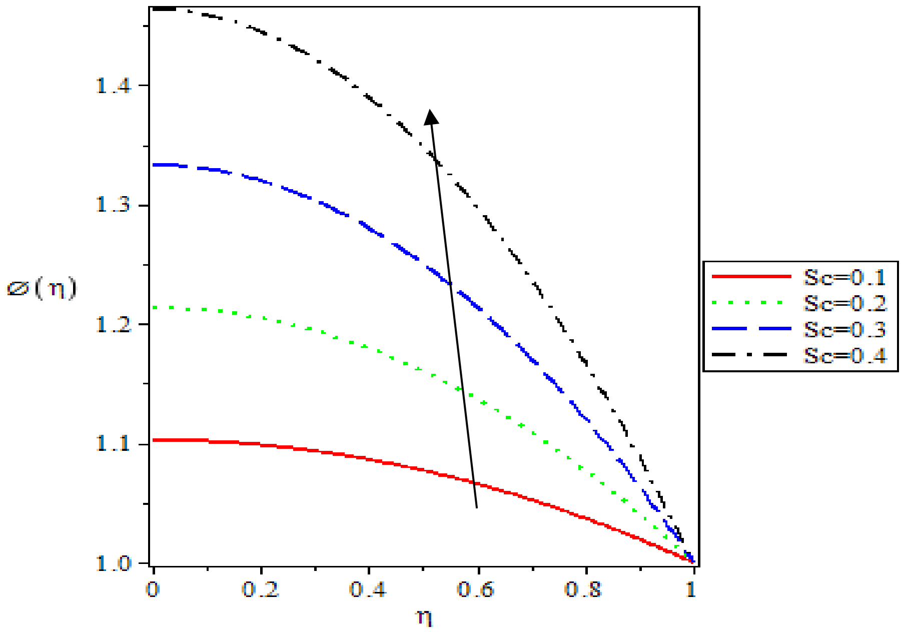

Figure 8. Influence of Sc on concentration profile

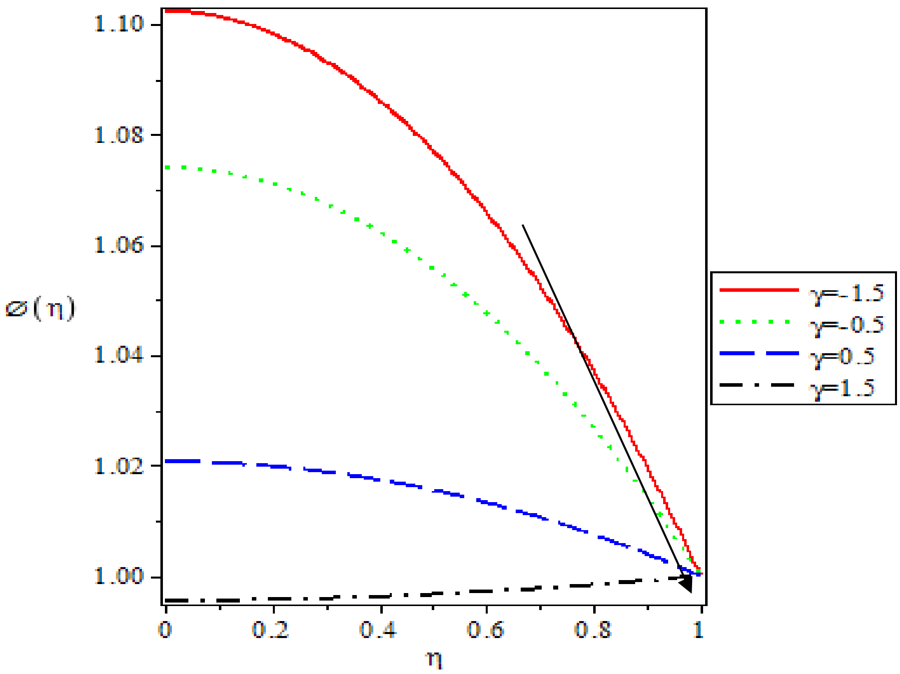

Figure 9. Influence of γ on the concentration profile

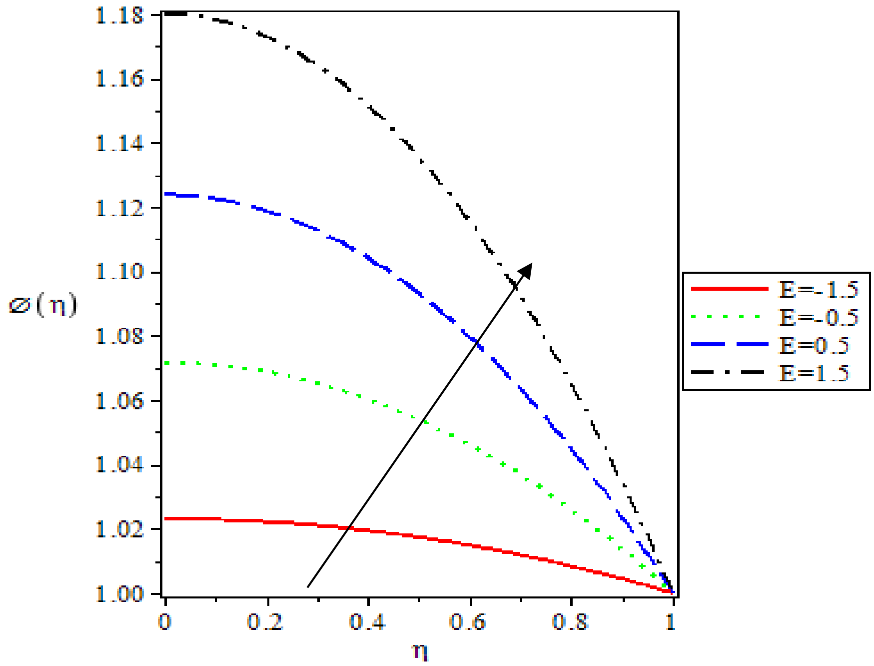

Figure 10. Influence of E on the concentration profile

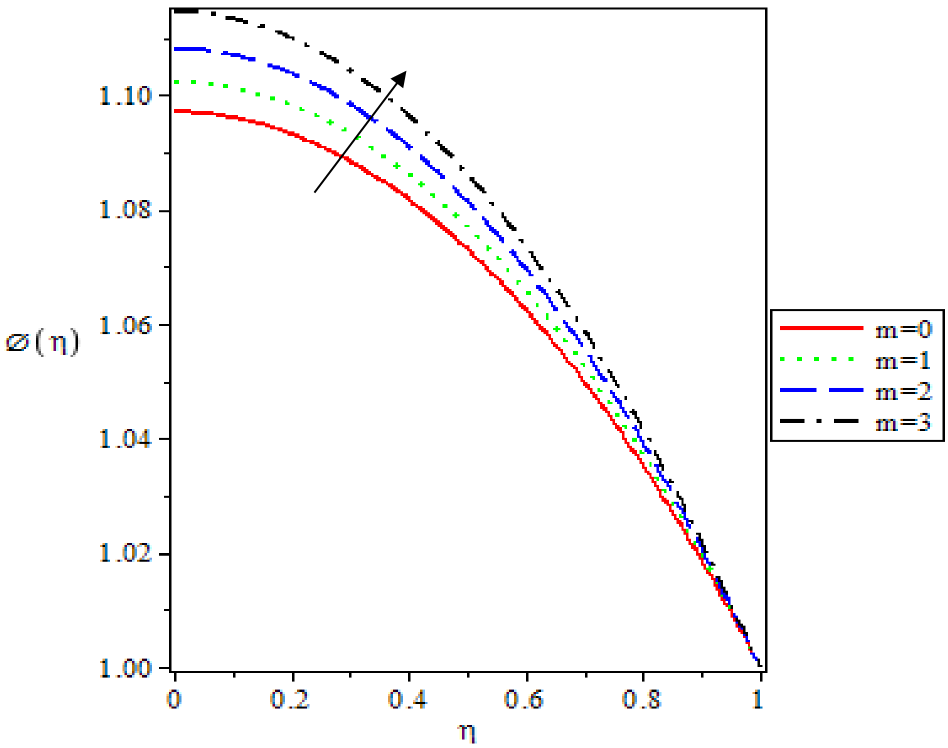

Figure 11. Influence of m on the concentration profile

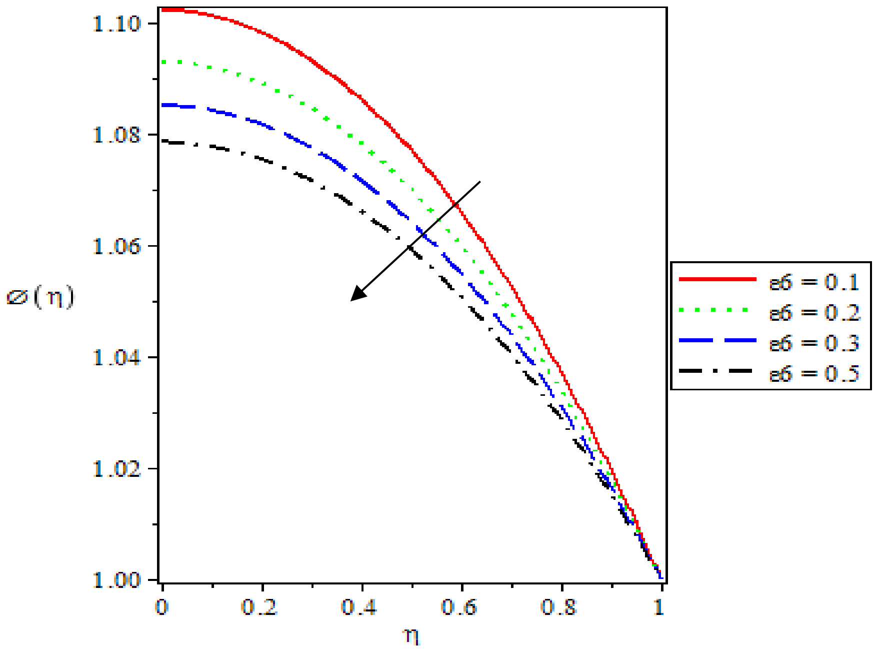

Figure 12. Influence of $\varepsilon_6$on the concentration profile

6. CONCLUSION

A hybrid numerical technique based on Chebyshev polynomials, the Galerkin formulation, and Gaussian quadrature integration was successfully employed to analyze the unsteady squeezing magnetohydrodynamic flow of an Eyring–Powell fluid with variable thermophysical properties. The results show that increasing electrical conductivity strengthens magnetic field effects, generating a resistive Lorentz force that suppresses fluid velocity within the flow domain. Furthermore, enhanced thermal conductivity improves heat transport, increasing temperature distribution and heat-transfer efficiency. The study also demonstrates that variable mass diffusivity significantly enhances species transport within the boundary layer, thereby increasing concentration levels. In addition, including Arrhenius activation energy reduces the effective chemical reaction rate by increasing the energy barrier required for molecular reactions, which consequently results in a higher concentration of unreacted species within the fluid. Overall, the findings provide important insight into the combined influence of magnetic field effects, non-Newtonian fluid behavior, and variable transport properties on momentum, heat, and mass transfer processes in squeezing flow systems.

REFERENCES

[1] P. A. Davidson, An Introduction to Magnetohydrodynamics. Cambridge, U.K.: Cambridge University Press, 2001.

[2] J. A. Shercliff, A Textbook of Magnetohydrodynamics. Oxford, U.K.: Pergamon Press, 1965.

[3] O. D. Makinde, "MHD boundary layer flow with heat transfer," *Int. J. Therm. Sci.*, vol. 50, no. 7, pp. 1326–1332, 2011. https://doi.org/10.1016/j.ijthermalsci.2011.02.019

[4] M. Sheikholeslami, "Numerical simulation of MHD nanofluid flow and heat transfer," *Int. J. Heat Mass Transf.*, vol. 115, pp. 1203–1213, 2017. https://doi.org/10.1016/j.ijheatmasstransfer.2017.08.108

[5] Afaq, H., Azhar, E. and Kamran, A., "Modeling and analysis of heat transfer in Eyring–Powell fluids with magnetic and viscous dissipation: Applications to MHD systems Multiscale and Multidisciplinary Modeling," *Experiments and Design*, vol. 8, 168, 2025. https://doi.org/10.1007/s41939-025-00741-2

[6] Abel, M. S., and Mahesha, N. J. A. M. M., "Heat transfer in MHD viscoelastic fluid flow over a stretching sheet with variable thermal conductivity, non-uniform heat source and radiation," *Applied Mathematical Modelling*, vol. 32, no. 10, pp. 1965-1983, 2008. https://doi.org/10.1016/j.apm.2007.06.038

[7] S. Abbasbandy and T. Hayat, "Solution of the MHD flow of Eyring–Powell fluid over a stretching sheet," *Phys. Lett. A*, vol. 372, no. 5, pp. 731–734, 2008. https://doi.org/10.1016/j.physleta.2008.12.045

[8] S. Nadeem and R. Mehmood, "Effects of thermal radiation on MHD flow of a Powell–Eyring fluid," *J. Assoc. Arab Univ. Basic Appl. Sci.*, vol. 13, pp. 1–8, 2013.

[9] T. Hayat, M. Imtiaz, and A. Alsaedi, "MHD flow of Eyring–Powell fluid with nonlinear thermal radiation," *J. Mol. Liq.*, vol. 215, pp. 152–159, 2016.

[10] T. Hayat, S. Nadeem, and A. Alsaedi, "MHD flow of Powell–Eyring nanofluid in porous medium with chemical reaction effects," *Results in Physics*, vol. 56, p. 107234, 2024.

[11] M. M. Rashidi, N. Freidoonimehr, and E. Momoniat, "Analytical solution of MHD boundary layer flow of non-Newtonian fluid," *Commun. Nonlinear Sci. Numer. Simul.*, vol. 19, no. 1, pp. 20–33, 2014.

[12] T. Hayat, M. Awais, and A. Alsaedi, “MHD flow of non-Newtonian fluid with heat transfer,” *Appl. Math. Comput*., vol. 217, no. 16, pp. 7066–7075, 2011.
[13] S. Nadeem and C. Fetecau, “Peristaltic transport of Eyring–Powell fluid under MHD effects with heat and mass transfer,” *International Journal of Heat and Mass Transfer*, vol. 215, p. 124567, 2024
[14] S. Nadeem, T. Hayat, and M. Imran, “Peristaltic flow of a non-Newtonian fluid in a channel,” *Appl. Math. Mech.*, vol. 35, no. 1, pp. 1–16, 2014.
[15] A. J. Chamkha, Z. Shah, and P. Kumari, “Variable viscosity and Arrhenius activation energy effects in MHD nanofluid flow,” *Applied Mathematical Modelling*, vol. 128, pp. 345–362, 2024.
[16] M. Sheikholeslami and D. D. Ganji, “MHD squeezing flow of nanofluid between parallel plates,” *Powder Technol.,* vol. 301, pp. 1102–1111, 2016.
[17] M. M. Rashidi, N. Freidoonimehr, and E. Momoniat, “Squeezing flow of a nanofluid between parallel plates,” *J. Mol. Liq.*, vol. 216, pp. 699–706, 2016.
[18] M. Sheikholeslami, “Influence of magnetic field on squeezing flow of nanofluid,” *Powder Technol*., vol. 322, pp. 135–143, 2017.
[19] S. U. Khan, T. Muhammad, and A. Alzahrani, “Chemical reaction and activation energy effects on Powell–Eyring nanofluid flow with heterogeneous–homogeneous reactions,” *Scientific Reports*, vol. 13, p. 18945, 2023.
[20] S. U. S. Choi and J. A. Eastman, “Enhancing thermal conductivity of fluids with nanoparticles,” *Proc. ASME Int. Mech. Eng. Congr. Expo.*, 1995. https://doi.org/10.1115/IMECE1995-0926
[21] A. Pantokratoras, “Variable viscosity effects on boundary layer flow,” *Appl. Math. Model.*, vol. 28, no. 5, pp. 431–440, 2004.
[22] Z. Abbas, I. Khan, and S. Islam, “Spectral collocation analysis of MHD Eyring–Powell dissipative flow over a stretching sheet,” *Computers & Fluids*, vol. 270, p. 106145, 2024.
[23] M. A. Seddeek, “Effects of radiation and variable viscosity on MHD flow,” *Int. Commun. Heat Mass Transf.*, vol. 29, no. 3, pp. 379–388, 2002.
[24] M. Sheikholeslami and A. M. Rashidi, “Unsteady MHD squeezing flow with chemical reaction and radiation effects in a channel,” *International Communications in Heat and Mass Transfer*, vol. 150, p. 107215, 2026.
[25] T. Hayat, Z. Iqbal, and A. Alsaedi, “Impact of variable thermal conductivity in MHD flows,” *Appl. Math. Mech.*, vol. 34, no. 2, pp. 123–138, 2013. https://doi.org/10.1007/s10483-013-1710-7
[26] M. M. Rashidi and N. Freidoonimehr, “Effects of chemical reaction on MHD flow,” *J. Taiwan Inst. Chem. Eng.*, vol. 45, no. 4, pp. 1658–1664, 2014.
[27] T. Hayat, S. A. Shehzad, and A. Alsaedi, “Effects of activation energy on MHD flow with chemical reaction,” *J. Mol. Liq.*, vol. 221, pp. 245–253, 2016.
[28] M. Sheikholeslami, T. Hayat, and S. Qayyum, “Thermosolutal convection of Powell–Eyring fluid in microchannel under magnetic field effects,” *Physics of Fluids*, vol. 36, p. 043102, 2024.
[29] O. D. Makinde, “MHD flow with heat and mass transfer,” *Int. J. Therm. Sci.*, vol. 50, no. 7, pp. 1326–1332, 2011.
[30] A. J. Chamkha and T. Hayat, “Variable property Powell–Eyring fluid flow with rotation and heat transfer effects,”*Journal of Non-Newtonian Fluid Mechanics*, vol. 335, p. 105392, 2024.
[31] M. Sheikholeslami, “Numerical modeling of MHD nanofluid flow with entropy generation,” *Phys. Fluids*, vol. 32, 2020.
[32] T. Hayat, A. Alsaedi, and M. Khan, “MHD flow of non-Newtonian fluids with thermal radiation,” *J. Mol. Liq.*, vol. 318, 2020.
[33] S. Nadeem et al., “Impact of activation energy on MHD nanofluid flow,” Case Stud. Therm. Eng., vol. 28, 2021.
[34] G. H. Author et al., “Variable thermal conductivity effects in nanofluid MHD boundary layer flows,” *Vubeta Journal of Computational Sciences*, 2024.
[35] M. Imran et al., “Numerical study of Eyring–Powell fluid with heat transfer,” *Results Eng.*, vol. 10, 2021.
[36] S. A. Obalalu, A. B. Adeyemi, and F. O. Akinola, “Numerical solution of Eyring–Powell MHD squeezing flow,” *Journal of Applied Fluid Mechanics*, vol. 10, no. 3, pp. 245–261, 2017.
[37] S. S. Ghadikolaei, M. N. Reza, and D. D. Ganji, “Analysis of unsteady MHD Eyring–Powell squeezing flow in stretching channel with thermal radiation and Joule heating,” *Case Studies in Thermal Engineering*, vol. 10, pp. 579–594, 2017. https://doi.org/10.1016/j.csite.2017.11.004
[38] I. J. Author and K. L. Author, “Activation energy and chemical reaction effects on squeezing channel flows,” *Vubeta Journal of Fluid Mechanics and Industrial Applications*, 2023.
[39] A. O. Author and B. O. Author, “MHD squeezing flow of non-Newtonian fluids in porous media with heat transfer effects,” *Vubeta Journal of Applied Mathematics and Mechanics*, 2023.
[40] C. D. Author and E. F. Author, “Numerical simulation of Eyring–Powell fluid flow under magnetic field influence,” *Vubeta International Journal of Engineering Research*, 2022.
[41] T. Hayat, S. Nadeem, and M. Imran, “Flow of an Eyring–Powell fluid over a stretching surface with heat transfer,” *Int. J. Heat Mass Transf.*, vol. 55, no. 11–12, pp. 3031–3038, 2012.
[42] J. P. Boyd, Chebyshev and Fourier Spectral Methods, 2nd ed. New York, NY, USA: Dover, 2001.
[43] C. Canuto, M. Y. Hussaini, A. Quarteroni, and T. A. Zang, Spectral Methods in Fluid Dynamics. Berlin, Germany: *Springer*, 1988. https://doi.org/10.1007/978-3-642-84108-8
[44] R. Peyret, Spectral Methods for Incompressible Flows. New York, NY, USA: Springer, 2002. https://doi.org/10.1007/978-1-4757-6557-1
[45] L. N. Trefethen, Spectral Methods in MATLAB. Philadelphia, PA, USA: SIAM, 2000. https://doi.org/10.1137/1.9780898719598

.

[46] D. Gottlieb and S. A. Orszag, Numerical Analysis of Spectral Methods. Philadelphia, PA, USA: SIAM, 1977. https://doi.org/10.1137/1.9781611970425

[47] S. A. Obalalu, A. R. Ismail, and S. Khan, "Chebyshev collocation method for solving boundary layer problems," *Applied Mathematics and Computation*, vol. 315, pp. 512–525, 2018.

[48] Acosta-Zamora, K. P., and Núñez, J., "On the solutions of fluid flow problems with a Chebyshev collocation method using Mathematica. Computer Applications in Engineering Education," vol. 30, no. 4, pp.1222-1235, 2022. https://doi.org/10.1002/cae.22516

[49] Alao, et al., "Weighted residual method for the squeezing flow between parallel walls plates, Americal International," *Journal of Research in Science, Technology, Engineering and Mathematic,* vol. 4, 2017. https://doi.org/10.30538/oms

[50] Akolade, M. T., and Idowu, A. S., "Radiation convection flow of Eyring–Powell Prandtl Eyring nanofluid over a convectively heated surface with thermo-chemical flux interactions," *Multiscale and Multidisciplinary Modeling*, Experiments and Design, vol. 8, no. 2, 140, 2025. https://doi.org/10.1007/s41939-024-00715-w

[51] Alhazmi et al., "A multi-layer neural network-based evaluation of MHD radiative heat transfer in Eyring–Powell fluid model", *Heliyon*, vol. 11, no. 3. 2025. https://doi.org/10.1016/j.heliyon.2025.e41800

[52] Alghamdi, et al., "Double layered combined convective heated flow of Eyring–Powell fluid across an elevated stretched cylinder using intelligent computing approach," *Case Studies in Thermal Engineering*, vol. 54, 104009, 2024. https://doi.org/10.1016/j.csite.2024.104009